Nuclear isospin mixing and elastic parity-violating electron scattering

O. Moreno,[1] P. Sarriguren,[1] E. Moya de Guerra,[2] J.M. Udias,[2] T.W. Donnelly,[3] and I. Sick[4]

[1]*Instituto de Estructura de la Materia, CSIC, Serrano 123, E-28006 Madrid, Spain*
[2]*Departamento de Física Atómica, Molecular y Nuclear, Universidad Complutense de Madrid,*
E-28040 Madrid, Spain
[3]*Center for Theoretical Physics, Laboratory for Nuclear Science and Department of Physics,*
Massachusetts Institute of Technology, Cambridge, MA 02139, USA
[4]*Departement für Physik, Universität Basel, CH-4056 Basel, Switzerland*

The influence of nuclear isospin mixing on parity-violating elastic electron scattering is studied for the even-even, $N = Z$ nuclei ^{12}C, ^{24}Mg, ^{28}Si, and ^{32}S. Their ground-state wave functions have been obtained using a self-consistent axially-symmetric mean-field approximation with density-dependent effective two-body Skyrme interactions. Some differences from previous shell-model calculations appear for the isovector Coulomb form factors which play a role in determining the parity-violating asymmetry. To gain an understanding of how these differences arise, the results have been expanded in a spherical harmonic oscillator basis. Results are obtained not only within the plane-wave Born approximation, but also using the distorted-wave Born approximation for comparison with potential future experimental studies of parity-violating electron scattering. To this end, for each nucleus the focus is placed on kinematic ranges where the signal (isospin-mixing effects on the parity-violating asymmetry) and the experimental figure-of-merit are maximized. Strangeness contributions to the asymmetry are also briefly discussed, since they and the isospin mixing contributions may play comparable roles for the nuclei being studied at the low momentum transfers of interest in the present work.

PACS numbers: 24.80.+y, 25.30.Bf, 21.60.Jz

I. INTRODUCTION

One motivation for studying parity-violating (PV) electron scattering from nuclei is to use it as a tool to extract information on the weak neutral current (WNC) and thereby to test the validity of the Standard Model in the low-energy regime [1, 2] (see also [3, 4]). This possibility lies in the fact that the PV asymmetry acquires a very simple, model-independent expression in terms of basic coupling constants, with nuclear structure effects cancelling out, if certain conditions are met. The assumptions required to arrive to such a simple expression are: (1) that the focus is placed on elastic scattering from spin-zero nuclear targets, for then only Coulomb-type monopole form factors enter; (2) that strangeness content in the WNC can be neglected, for then only isoscalar and isovector matrix elements occur, with no third type of contribution; and (3) that the nuclear ground states have isospin zero, permitting only a single Coulomb monopole matrix element to occur, namely, the isoscalar one. In fact, while restriction (1) can be met with a wide range of even-even nuclei, restrictions (2) and (3) are not completely attainable. Strangeness content in the WNC has been extensively studied in previous work (see, for instance, the review article [4]) and is not the primary focus of the present study. Instead, the present work is aimed at the last issue of potential isospin mixing in nuclear ground states and how this affects the PV asymmetry, albeit taking into account present uncertainties in the strangeness content of the nucleon.

Isospin mixing constituted part of the goal of a previous study by Donnelly, Dubach and Sick (DDS) [5] where the effect of isospin mixing in nuclear ground states on PV electron scattering was first studied. The approach taken there was to use a simple two-level model in which the $T = 0$ ground state and an excited $T = 1$ state, both with angular momentum/parity 0^+, were admixed with a mixing parameter χ. The deviation in the PV asymmetry due to isospin mixing was found to be proportional to this mixing parameter χ and to the ratio between the inelastic isovector and the elastic isoscalar Coulomb monopole form factors. In DDS a shell-model approach with only one active shell in a spherical harmonic oscillator basis was used to obtain the spin-isospin reduced Coulomb matrix elements (isoscalar and isovector) for ^{12}C and ^{28}Si. Coulomb distortion effects on the electron waves were also neglected in that earlier work.

Isospin dependence in PV electron scattering is crucial in attempting to determine the precision up to which the Standard Model constants can be deduced and to what extent strangeness effects in the WNC can be studied. At the same time, this dependence can be exploited to provide information about the spatial distribution of neutrons in the nuclear ground state. Indeed, this idea was proposed as part of the original study by DDS, namely that a measurement of the electron-scattering PV-asymmetry can provide a direct measurement of the Fourier Transform of the neutron density. In a subsequent study [6] the idea in DDS was extended to allow for Coulomb distortion of the electron wave function, something also done in the present work. Neutron densities are less well known than charge

densities (studied using parity-conserving electron scattering) as most of this information comes from hadronic probes where the reaction mechanism involved is more difficult to interpret than is the case for semi-leptonic electroweak processes. Thus, an electroweak measurement of the neutron density can serve to calibrate the measurements made with hadronic probes. In fact, the idea proposed by DDS is now being realized in the Parity Radius Experiment (PREX) at Jefferson Laboratory which has the goal of measuring the neutron radius of ^{208}Pb using PV elastic electron scattering. Such a measurement has implications for astrophysics (including the structure of neutron stars), for atomic parity non-conservation studies, for the structure of neutron-rich nuclei, and for determinations of neutron skin thicknesses of nuclei.

In this work we extend the previous study undertaken by DDS to examine the effects on the PV asymmetry induced by isospin admixtures in the nuclear ground states of N=Z nuclei occurring when Coulomb interactions between nucleons are taken into account and pairing correlations are included. The nuclear structure is described within a self-consistent axially-symmetric Hartree-Fock formalism with Skyrme forces; in fact, three different forces are used to explore the sensitivity of the PV asymmetry deviation to the nuclear dynamics. Several additional extensions beyond the work of DDS are made, namely, inclusion of the spin-orbit correction to the Coulomb monopole operators, use of modern electroweak form factors for protons and neutrons, inclusion of strangeness contributions in the nucleon form factors, and, as noted above, incorporation of the effects caused by the Coulomb distortion of the electron wave functions. The present study includes four N=Z isotopes, namely, ^{12}C, ^{24}Mg, ^{28}Si, and ^{32}S.

With respect to nuclear structure issues, the main difference between the treatment in DDS and here is that in DDS Coulomb effects in the nuclear ground state are considered perturbatively to find the admixture of giant isovector monopole strength ($J = 0^+$, $T = 1$), as explained at length in [7]. Here, within the self-consistent mean-field approach with two-body density-dependent effective interactions, the collective isospin mixing effect of the Coulomb force is included non-perturbatively in the isospin-non-conserving Hartree-Fock (HF) mean field, along with other collective effects such as pairing and deformation. As a result, the HF+BCS ground state is made up of quasiparticles with rather complex admixtures of harmonic oscillator wave functions in many different major shells.

In discussing the results one sees that there are limited kinematical regions where the PV asymmetry is measurable at the levels required, i.e., as characterized by the figure-of-merit (FOM) which typically peaks at momentum transfers around 0.5 fm^{-1}. For the region extending up to a little beyond 1 fm^{-1} the effects of isospin mixing on the PV asymmetry will be seen later to be characteristically at the level of a few percent for light nuclei, up to more than 10% for the heavier nuclei considered. These are certainly within the scope of existing and future measurements of PV electron scattering. For example, the HAPPEX-He measurements at JLab [8] have already been performed at low q, i.e., for kinematics similar to those of relevance in the present work. These yielded PV asymmetries at the 4% level (which are statistically, not systematically limited at present), while the future PREX measurements on Pb [9] aim for 3% precision in the PV asymmetry. In fact, in recent work (see [10] and references therein) it has been noted that interpretations of results from experiments like HAPPEX and G0 are reaching the point where they are limited by effects from isospin mixing. For heavier nuclei, as discussed in the present work, the effects from isospin mixing will be seen to be even larger than for the nucleon or few-body nuclei.

At higher momentum transfers the effects of isospin mixing are still larger; however, the FOM is smaller in this region and, as a consequence, our attention in the present work is focused only on the lower momentum transfer region. As far as other contributions are concerned, after discussing our basic results, and thereby setting the scale of the isospin mixing, we return briefly to show the size of potential strangeness effects and of the expected influence of meson-exchange currents at these lower momentum transfers. Other effects such as parity admixtures in the nuclear ground state, dispersion corrections, or radiative corrections are expected to provide negligible modifications to the asymmetry [6] and are not considered in this work.

The outline of the paper is the following. In Sect. II we start by introducing the formalism necessary to describe PV in polarized elastic electron scattering from spin-zero N=Z nuclei. The correction to the asymmetry due to isospin mixing is isolated and analyzed in terms of the various ingredients involved, such as the roles played by the nucleon form factors and by potential strangeness contributions. There we also discuss the effects expected from electron distortions. In Sect. III we present our results on the PV asymmetry for the four nuclei under study. First we explore the influence on the results of the various ingredients in the formalism (different pairing gaps, different Skyrme interactions, the spin-orbit correction) and go on to compare the present work with past studies of isospin-mixing effects in PV electron scattering. Following this, the principal results of the study are presented for the four chosen nuclei and finally, in Sect. IV, we summarize the main conclusions of our work.

II. FORMALISM

A. Parity-violation asymmetry

Polarized single-arm electron scattering from unpolarized nuclei can be used to study parity violation, since both electromagnetic (EM) and weak interactions contribute to the process via γ and Z^0 exchange, respectively. The PV asymmetry is given by [4]

$$\mathcal{A} = \frac{d\sigma^+ - d\sigma^-}{d\sigma^+ + d\sigma^-}, \tag{1}$$

where $d\sigma^+(d\sigma^-)$ is the cross section for electrons longitudinally polarized parallel (antiparallel) to their momentum. Keeping only the square of the photon-exchange amplitude for the spin-averaged EM cross section and using the interference between the γ and Z^0 amplitudes in the cross section difference, in Plane Wave Born Approximation (PWBA) the asymmetry $\mathcal{A}$ in the Standard Model can be written as

$$\mathcal{A} = \frac{G}{2\pi\alpha\sqrt{2}}|Q^2|\frac{W^{PV}}{F^2}, \tag{2}$$

where G and α are the Fermi and fine-structure coupling constants, respectively, and Q is the four-momentum transfer in the scattering process. W^{PV} is the PV response and F is the EM form factor, both containing the dependence of the asymmetry on the nuclear structure. In the case of elastic electron scattering between $J^\pi = 0^+$ states, only the Coulomb-type monopole operators can induce the transition,

$$F^2(q) = v_L F_{C0}^2(q), \quad W^{PV} = v_L a_A F_{C0}(q)\tilde{F}_{C0}(q), \tag{3}$$

where $a_A = -1$, v_L is a kinematical factor that cancels out in the ratio, and $F_{C0}(\tilde{F}_{C0})$ is the EM(WNC) monopole Coulomb form factor. Then one has

$$\frac{W^{PV}}{F^2} = a_A \frac{\tilde{F}_{C0}(q)}{F_{C0}(q)}. \tag{4}$$

If we now consider only $N = Z$ nuclei and assume that they are isospin eigenstates with isospin zero in their ground states, then only isoscalar matrix elements contribute and the weak and EM form factors become proportional:

$$\tilde{F}_{C0}(q) = \beta_V^{(0)} F_{C0}(q). \tag{5}$$

Accordingly, the PV asymmetry does not depend on the form factors:

$$\mathcal{A} = \mathcal{A}^0 \equiv \left[\frac{G|Q^2|}{2\pi\alpha\sqrt{2}}\right] a_A \beta_V^{(0)} \cong 3.22 \times 10^{-6}|Q^2| \text{ (in fm}^{-2}), \tag{6}$$

where, within the Standard Model, $a_A\beta_V^{(0)} = 2\sin^2\theta_W$, θ_W being the weak mixing angle.

The actual PV asymmetry deviates from this constant value by a correction Γ, where

$$\mathcal{A} = \mathcal{A}^0(1 + \Gamma) \tag{7}$$

or equivalently (for $J^\pi = 0^+$ nuclei)

$$\Gamma = \frac{1}{\beta_V^{(0)}} \frac{\tilde{F}_{C0}(q)}{F_{C0}(q)} - 1 \tag{8}$$

and it accounts, in particular, for the effects of nuclear isospin mixing and strangeness content in the PV asymmetry. The ratio between the WNC and EM form factors can be written as

$$\frac{\tilde{F}_{C0}(q)}{F_{C0}(q)} = \frac{\beta_V^{(0)}\langle 0||M_{0\,(T=0)}^C(q)||0\rangle + \beta_V^{(1)}\langle 0||M_{0\,(T=1)}^C(q)||0\rangle}{\langle 0||M_{0\,(T=0)}^C(q)||0\rangle + \langle 0||M_{0\,(T=1)}^C(q)||0\rangle}, \tag{9}$$

where the subscript in parenthesis indicates isoscalar ($T = 0$) and isovector ($T = 1$) parts.

The Coulomb isoscalar ($T = 0$) and isovector ($T = 1$) multipole operators can be written in terms of the contributions of order 0 and 1 in $\eta = p/m_N$ (subscripts (0) and (1)) [11, 12, 13]:

$$M_J^{C\,M_J}(q\mathbf{x}) = M_J^{C\,M_J}(q\mathbf{x})_{(0)} + M_J^{C\,M_J}(q\mathbf{x})_{(1)} \,. \tag{10}$$

The nucleon form factors G_E and G_M are included in the definitions of the two contributions as follows:

$$M_J^{C\,M_J}(q\mathbf{x})_{(0)} = \frac{\kappa}{\sqrt{\tau}} G_E(\tau) M_J^{M_J}(q\mathbf{x})\,, \tag{11}$$

$$M_J^{C\,M_J}(q\mathbf{x})_{(1)} = \kappa\sqrt{\tau}\,[2G_M(\tau) - G_E(\tau)]\,\Theta_J^{M_J}(q\mathbf{x})\,, \tag{12}$$

where the kinematical factors κ and τ contain the energy ω and momentum q transferred to the nucleus by the electron:

$$\kappa = \frac{q}{2m_N}\,, \qquad \tau = \frac{|Q^2|}{4m_N^2} = \frac{q^2 - \omega^2}{4m_N^2}\,, \tag{13}$$

and $G_{E(M)}$ are the electric (magnetic) nucleon form factors discussed later. The basic multipole operators $M_J^{M_J}$ and $\Theta_J^{M_J}$ are respectively the standard zeroth-order Coulomb operator and the spin-orbit first-order correction, and are defined as:

$$M_J^{M_J}(q\mathbf{x}) = j_J(q\mathbf{x}) Y_J^{M_J}(\hat{\mathbf{x}})\,, \tag{14}$$

$$\Theta_J^{M_J}(q\mathbf{x}) = -\frac{i}{q^2}\vec{\sigma}\cdot\left[\left(\vec{\nabla} M_J^{M_J}(q\mathbf{x}) \times \vec{\nabla}\right)\right]\,. \tag{15}$$

By using the relations between form factors in isospin space ($T = 0, 1$) and form factors in charge space (proton:p and neutron:n),

$$M_{J\,(T=0)}^{C\,M_J} = M_{J\,(p)}^{C\,M_J} + M_{J\,(n)}^{C\,M_J}\,, \tag{16}$$

$$M_{J\,(T=1)}^{C\,M_J} = M_{J\,(p)}^{C\,M_J} - M_{J\,(n)}^{C\,M_J}\,, \tag{17}$$

$$G_E^{(0)} = G_{E_p} + G_{E_n}\,, \tag{18}$$

$$G_E^{(1)} = G_{E_p} - G_{E_n}\,, \tag{19}$$

$$G_M^{(0)} = G_{M_p} + G_{M_n}\,, \tag{20}$$

$$G_M^{(1)} = G_{M_p} - G_{M_n}\,, \tag{21}$$

$$\tag{22}$$

one can write the ratio in Eq. (9) as

$$\frac{\widetilde{F}_{C0}(q)}{F_{C0}(q)} = \frac{\langle 0||\widetilde{M}_{0\,(p)}^C(q)||0\rangle + \langle 0||\widetilde{M}_{0\,(n)}^C(q)||0\rangle}{\langle 0||M_{0\,(p)}^C(q)||0\rangle + \langle 0||M_{0\,(n)}^C(q)||0\rangle}\,, \tag{23}$$

where the operators with tildes, $\widetilde{M}$, have the same structure as in Eqs. (10, 11), but contain the WNC nucleon form factors $\widetilde{G}_E$, $\widetilde{G}_M$ to be defined in the next subsection.

In the present study we are interested in the $J = 0$ ($M_J=0$) multipole. The charge operator M_0^0 matrix elements in a spherical harmonic oscillator (s.h.o.) basis are given by

$$\langle n'l'j'|M_0^0(q\mathbf{x})|nlj\rangle = \frac{1}{\sqrt{4\pi}}\,\langle n'l'j'|j_0(qr)|nlj\rangle\,\delta_{l'l}\,\delta_{j'j} = \frac{1}{\sqrt{4\pi}}\int j_0(qr)\,R_{nl}(r)R_{n'l}(r)\,r^2\,dr\,. \tag{24}$$

For $J = 0$ the spin-orbit operator Θ_0^0 is just proportional to $\vec{l}\cdot\vec{s}$ and one has in the same s.h.o. basis:

$$\langle n'l'j'|\Theta_0^0(q\mathbf{x})|nlj\rangle = -\frac{1}{\sqrt{4\pi}}\frac{1}{2}\left[j(j+1) - l(l+1) - \frac{3}{4}\right]\left\langle n'l'j'\left|\frac{j_1(qr)}{qr}\right|nlj\right\rangle\delta_{l'l}\,\delta_{j'j} = \tag{25}$$

$$-\frac{1}{\sqrt{4\pi}}\frac{1}{2}\left[j(j+1) - l(l+1) - \frac{3}{4}\right]\int\frac{j_1(qr)}{qr}\,R_{nl}(r)R_{n'l}(r)\,r^2\,dr\,.$$

In both expressions $j_\lambda(qr)$ is a spherical Bessel function of order λ. The matrix elements of the charge monopole operators (EM and WNC) between two s.h.o. wave functions are therefore

$$
\begin{aligned}
f^\xi_{nn'lj}(q) &\equiv \langle n'lj|M^{C\,0}_{0\,(\xi)}(q\mathbf{x})|nlj\rangle \\
&= \frac{\kappa}{\sqrt{\tau}}G_{E_\xi}(\tau)\langle n'lj|M^0_0(q\mathbf{x})|nlj\rangle + \kappa\sqrt{\tau}\left[2G_{M_\xi}(\tau)-G_{E_\xi}(\tau)\right]\langle n'lj|\Theta^0_0(q\mathbf{x})|nlj\rangle
\end{aligned}
\tag{26}
$$

$$
\begin{aligned}
\widetilde{f}^\xi_{nn'lj}(q) &\equiv \langle n'lj|\widetilde{M}^{C\,0}_{0\,(\xi)}(q\mathbf{x})|nlj\rangle \\
&= \frac{\kappa}{\sqrt{\tau}}\widetilde{G}_{E_\xi}(\tau)\langle n'lj|M^0_0(q\mathbf{x})|nlj\rangle + \kappa\sqrt{\tau}\left[2\widetilde{G}_{M_\xi}(\tau)-\widetilde{G}_{E_\xi}(\tau)\right]\langle n'lj|\Theta^0_0(q\mathbf{x})|nlj\rangle\,,
\end{aligned}
\tag{27}
$$

where the proton ($\xi = p$ or π) and neutron ($\xi = n$ or ν) form factors G and $\widetilde{G}$ will be defined in the next subsection. Note that one should not confuse n as a superscript on f and $\widetilde{f}$ meaning neutron with n as a subscript meaning the quantum number labeling the single-particle basis states — the context will also make the distinction clear. The expressions above are used once the s.h.o. expansion of the HF single-particle wave functions is performed (see below). The total monopole matrix elements also contain a center-of-mass correction factor to account for the fact that the HF single-particle wave functions are referred to the center of the mean-field potential, not to the nuclear center of mass, as they should be to avoid the spurious movement of the nucleus as a whole. For a s.h.o. potential, this correction factor takes the form $f_{CM} = \exp(q^2 b^2/4A) \cong \exp(q^2/4A^{2/3})$, with q the momentum transfer (in fm^{-1}), b the oscillator parameter (in fm) and A the total number of nucleons. This is usually employed even when not using a s.h.o. basis; the correction cancels out when one constructs the ratios of form factors appearing in the asymmetry $\mathcal{A}$.

Finally, let us conclude this section with a brief discussion of potential meson-exchange current effects on the PV asymmetry (see also [4]). Such contributions enter in very different ways in cross sections and in the asymmetry. In the former they typically provide effects at the few percent level, whereas for the latter the situation is not so obvious. First, were there to be no significant isospin mixing and strangeness contributions, i.e., with a purely isoscalar, no-strangeness ground state, then the MEC effects would cancel in the ratio that gives the PV asymmetry, and, in fact, the result would be completely unaffected by any aspect of hadronic structure. This is an old result [1, 2] from the earliest studies of elastic PV electron scattering from nuclei. Secondly, with isospin mixing the situation is more complicated, since now there are both isoscalar and isovector electromagnetic current matrix elements involved and MEC effects are different for the two. However, two arguments suggest that these contributions are not significant for the present study at low momentum transfers: the multipoles involved are C0 (isoscalar and isovector) where MEC effects, being dominantly transverse, are suppressed anyway and the effect is one of modifying the predicted isovector effect from occurring as a purely one-body matrix element to one where both one-body and typically few percent two-body contributions occur. This would modify the isospin-mixing PV results by a multiplicative (not additive) factor of typically a few percent, which is not significant for the present study. Thirdly, with strangeness also present, now in the nucleon itself and also in MEC contributions, additional effects may occur. A study was done [14] for the important case of ^{4}He and, based on the results presented there, it may be that at higher values of q (beyond roughly 3 fm^{-1}) such effects could become significant. On the other hand, in the cited study such effects were shown to be negligible for the range of momentum transfers of interest in the present work and accordingly here we also neglect any contributions of this type.

B.   Nucleon form factors and strangeness

The electric nucleon form factor can be expressed either in terms of protons and neutrons or in terms of isoscalar and isovector parts,

$$
G_E = G_{E_p}\frac{1}{2}(1+\tau_3) + G_{E_n}\frac{1}{2}(1-\tau_3) = \frac{1}{2}(G^{(0)}_E + \tau_3 G^{(1)}_E)\,,
\tag{28}
$$

where τ_3 is 1 for protons and -1 for neutrons. In analogy, in the Standard Model, the WNC nucleon form factor is given by

$$
\widetilde{G}_E = \frac{1}{2}(\beta^{(0)}_V G^{(0)}_E + \beta^{(s)}_V G^{(s)}_E + \tau_3 \beta^{(1)}_V G^{(1)}_E)\,,
\tag{29}
$$

where the strangeness contribution to the form factor is isoscalar. This can also be written in terms of proton and neutron form factors,

$$
\widetilde{G}_E = \widetilde{G}_{E_p}\frac{1}{2}(1+\tau_3) + \widetilde{G}_{E_n}\frac{1}{2}(1-\tau_3)\,,
\tag{30}
$$

where

$$\widetilde{G}_{E_p} = \beta_V^p G_{E_p} + \beta_V^n G_{E_n} + \frac{1}{2}\beta_V^{(s)} G_E^{(s)} \,, \tag{31}$$

$$\widetilde{G}_{E_n} = \beta_V^n G_{E_p} + \beta_V^p G_{E_n} + \frac{1}{2}\beta_V^{(s)} G_E^{(s)} \,. \tag{32}$$

A similar result applies to the nucleon magnetic form factors by simply substituting G_E by G_M in the previous expressions. The nucleon form factors G_E and G_M, from which $\widetilde{G}_E$ and $\widetilde{G}_M$ are obtained, have been computed using the parametrization by Höhler [15].

Within the Standard Model we have,

$$\beta_V^{(0)} = \beta_V^p + \beta_V^n = -2\sin^2\theta_W = -0.46 \tag{33}$$

$$\beta_V^{(1)} = \beta_V^p - \beta_V^n = 1 - 2\sin^2\theta_W = 0.54 \tag{34}$$

$$\beta_V^p = \frac{1}{2}\left(\beta_V^{(0)} + \beta_V^{(1)}\right) = 0.04 \tag{35}$$

$$\beta_V^n = \frac{1}{2}\left(\beta_V^{(0)} - \beta_V^{(1)}\right) = -0.5 \tag{36}$$

$$\beta_V^{(s)} = -1 \tag{37}$$

The strangeness form factor $G_E^{(s)}$ has been parametrized according to

$$G_E^{(s)} = \rho_s \tau G_D^V \xi_E^{(s)}, \qquad G_M^{(s)} = \mu_s G_D^V \,, \tag{38}$$

(see, for instance, [4]) with

$$G_D^V = (1 + 4.97\tau)^{-2}, \quad \xi_E^{(s)} = (1 + 5.6\tau)^{-1} \,. \tag{39}$$

The parameters ρ_s and μ_s are constrained by PV electron scattering measurements on hydrogen, deuterium and helium-4; the values chosen as representative are discussed below and in Sect. III.

C. Contributions to the PV asymmetry

The strangeness term in the WNC form factors in Eq. (31) can be considered separately, giving rise to a decomposition of the PV asymmetry deviation, $\Gamma = \Gamma^{(I)} + \Gamma^{(s)}$, where the isospin mixing term $\Gamma^{(I)}$ is proportional to $\beta_V^{(1)}/\beta_V^{(0)}$ and $\Gamma^{(s)}$ is proportional to $\beta_V^{(s)}/\beta_V^{(0)}$. The isospin mixing piece is computed considering $G_E^{(s)} = 0$ and $G_M^{(s)} = 0$ in the WNC form factors, whereas the strangeness term is computed considering $G_{E_p} = 0$, $G_{E_n} = 0$, $G_{M_p} = 0$ and $G_{M_n} = 0$ in the WNC form factors.

We evaluate the strangeness contribution neglecting the small differences between neutron and proton densities, assuming $G_{E_n}=0$, and neglecting the small spin-orbit contribution so only $G_E^{(s)}$ enters and not $G_M^{(s)}$. This gives

$$\Gamma^{(s)} = \frac{\beta_V^{(s)}}{\beta_V^{(0)}} \frac{G_E^{(s)}}{G_E^{(0)}} \,. \tag{40}$$

Once we have introduced the nucleon form factors, it is interesting to notice that if one neglects the spin-orbit correction to the Coulomb operator, Eq. (12), one obtains the more intuitive expression

$$\frac{\widetilde{F}_{C0}(q)}{F_{C0}(q)} = \frac{\widetilde{G}_{E_p}\langle 0||M_{0\,(p)}(q)||0\rangle + \widetilde{G}_{E_n}\langle 0||M_{0\,(n)}(q)||0\rangle}{G_{E_p}\langle 0||M_{0\,(p)}(q)||0\rangle + G_{E_n}\langle 0||M_{0\,(n)}(q)||0\rangle} \,, \tag{41}$$

with

$$\langle 0||M_{0\,(\xi)}(q)||0\rangle \sim \int j_0(qr)\rho_{(\xi)}(r)r^2 dr \,, \tag{42}$$

where $\rho_{(\xi)}$ are the ground-state radial densities for protons and neutrons with ξ as above. If one further neglects the electric neutron form factor G_{En} and the strangeness form factors $G_E^{(s)}$, one arrives at the simple expression

$$\frac{\widetilde{F}_{C0}(q)}{F_{C0}(q)} = \beta_V^p + \beta_V^n \frac{\langle 0||M_{0\,(n)}(q)||0\rangle}{\langle 0||M_{0\,(p)}(q)||0\rangle}\,, \tag{43}$$

or equivalently

$$\Gamma = \frac{\beta_V^n}{\beta_V^{(0)}} \left(\frac{\langle 0||M_{0\,(n)}(q)||0\rangle - \langle 0||M_{0\,(p)}(q)||0\rangle}{\langle 0||M_{0\,(p)}(q)||0\rangle} \right) \tag{44}$$

which are similar to those used in DDS.

D. Kinematics and the figure-of-merit

As a general consideration, one faces a compromise between optimizing the PV signal (*i.e.*, deviations in the asymmetry) and the figure-of-merit, discussed below. Since the asymmetry generally increases with $|Q^2|$, while the cross section decreases, this leads to the search for a well defined region of optimal kinematics. To measure properly effects in the PV asymmetry due to isospin mixing, the deviation should be greater than or of the order of a few percent of the reference value $\mathcal{A}^0$ given in Eq. (6). This condition will be fulfilled in general for some intervals of q, but not for others. At the same time the relative error of the asymmetry should be kept as small as possible. This relative error depends on technical characteristics of the experimental setting (detector solid angle, beam luminosity and running time) gathered in X_0, as well as on intrinsic properties of the target, the projectile and their kinematics gathered in the so called figure-of-merit (FOM) $\mathcal{F}$ (see [4]):

$$\frac{\delta\mathcal{A}}{\mathcal{A}} = \frac{1}{\sqrt{\mathcal{F}\,X_0}}\,. \tag{45}$$

Clearly, in a study of the present type where the focus is placed on theoretical aspects of the hadronic and nuclear many-body physics in the problem, it is not appropriate to go into further detail on specific experimental conditions, *i.e.*, on the specifics of X_0 (see, however, [4] for some general discussions of experimental aspects of PV electron scattering). Presenting the FOM, as we do in the following section, provides a sufficient measure of the "doability" of PV elastic scattering asymmetry measurements whose goal is to explore isospin mixing in the nuclear ground state. In particular, the FOM is proportional to the asymmetry itself squared and to the differential cross section of the scattering (essentially the parity-conserving cross section):

$$\mathcal{F} = \frac{d\sigma}{d\Omega}\mathcal{A}^2\,, \tag{46}$$

and therefore shows a diffraction pattern, but with the same negative-slope trend as the differential cross section when the momentum transfer increases, which favors low momentum transfer experiments.

E. HF+BCS ground-state density

To generate the ground-state wave function in the HF+BCS approximation we use a Skyrme type density-dependent nucleon-nucleon interaction (SLy4 force [16]), allowing for axially-symmetric deformation. First, the HF equations are solved to generate the self-consistent HF mean field, and pairing correlations are taken into account at each iteration solving the BCS equations to generate the single quasiparticle wave functions. The deformed HF+BCS calculation gives a set of single-particle levels, occupation numbers, and wave functions Φ_{HF}^i. The latter are expanded in a deformed harmonic oscillator basis $\vartheta_{n_\rho n_z \Lambda \Sigma}$ which we also expand in a s.h.o. basis $\phi_{nlj(m_j)}$ to facilitate the comparison with previous work based on the shell-model approach,

$$\Phi_{HF}^i(\vec{r}) = \sum_{n_\rho n_z \Lambda \Sigma} k_{n_\rho n_z \Lambda \Sigma}^i \, \vartheta_{n_\rho n_z \Lambda \Sigma}(\vec{r}) = \sum_{nlj} c_{nlj}^i \, \phi_{nljm_j}(\vec{r})\,, \tag{47}$$

where a truncation of 11 major shells N has been used in both the deformed ($N = 2n_\rho + n_z + \Lambda$) and the spherical ($N = 2n + l$) expansions. Each HF single-particle state i has a parity and an angular momentum projection K^π which

are shared by any of the basis wave functions taking part in its expansion ($\pi = (-1)^l = (-1)^{n_z + \Lambda}$, $K = m_j = \Lambda + \Sigma$). The HF+BCS outputs give for every state i the energy, the occupation probability v_i^2 and the coefficients k^i. The coefficients in the s.h.o. basis expansion c_{nlj}^i are obtained as

$$c_{nlj}^i = \sum_{n_\rho n_z \Lambda \Sigma} k_{n_\rho n_z \Lambda \Sigma}^i C_{Nljm}^{n_\rho n_z \Lambda \Sigma}, \tag{48}$$

with

$$C_{Nljm}^{n_\rho n_z \Lambda \Sigma} = \langle l \, \tfrac{1}{2} \, \Lambda \, \Sigma \mid j \, m \rangle (-1)^\Lambda \sqrt{\frac{(2l+1)(l-\Lambda)!}{2(l+\Lambda)!}} \int r^2 dr R_{nl}(r) F(r) \tag{49}$$

and

$$F(r) = 2 \int_0^1 dt P_l^\Lambda(t) \psi_{n_\rho}^\Lambda (r^2(1-t^2)) \psi_{n_z}(rt), \tag{50}$$

where the P_l^Λ are associated Legendre polynomials and the functions ψ are defined in terms of Hermite and generalized Laguerre polynomials that contain, respectively, the cylindrical $z = rt$ and $\rho^2 = r^2(1-t^2)$ dependence of the eigenstates $\vartheta_{n_\rho n_z \Lambda \Sigma}(\vec{r})$ of the deformed harmonic oscillator potential [17, 18].

The contribution of each pair of s.h.o. states to the total charge monopole form factors (EM or WNC) can be analyzed in terms of two pieces as follows:

$$\langle 0 || M_{0\,(\xi)}^C(q) || 0 \rangle = \sum_{nn'lj} f_{nn'lj}^\xi(q) \, \rho_{nn'lj}^\xi, \tag{51}$$

$$\langle 0 || \widetilde{M}_{0\,(\xi)}^C(q) || 0 \rangle = \sum_{nn'lj} \widetilde{f}_{nn'lj}^\xi(q) \, \rho_{nn'lj}^\xi, \tag{52}$$

applicable to protons and neutrons ($\xi = p, \ n$) separately. The first factor in the above equations is the matrix element of the charge monopole operator (EM or WNC) between two s.h.o. states as defined in Eq. (26) or (27), which is momentum-dependent and whose j-dependence is only due to the spin-orbit correction (Eq. (25)). This matrix element vanishes unless both basis functions have the same lj quantum numbers. The nuclear ground-state structure information is contained in the second factor, which is the spherical part of the HF+BCS ground-state density matrix (for protons or neutrons) in the s.h.o. basis:

$$\rho_{nn'lj} = \sum_i 2v_i^2 \, c_{nlj}^i c_{n'lj}^i \ . \tag{53}$$

It contains the coefficients of pairs of spherical harmonic oscillator components differing at most in the radial quantum number n, as well as the occupation probabilities v_i^2 of each of the HF single-particle states i. These contributions are added up so that the calculated density refers to the whole HF+BCS ground state of the nucleus. The spherical density matrix elements contain information on the nuclear ground-state structure of the target isotopes. We note that the total HF+BCS density matrix may also contain a non-spherical part, with matrix elements $\rho_{nn'll'jj'}$, which for deformed nuclei is nonzero and which does not contribute to the charge monopole form factors. This ensures that only the spherically symmetric ($J = 0$) part of the neutron and proton densities contributes and that there is no need to make any further angular momentum projection in the deformed nuclei [19, 20]. The analysis of the quantities defined above is especially appropriate when comparing results of our HF+BCS calculations with former shell-model results, since each quasiparticle state can always be expressed as a combination of s.h.o. basis states with different radial quantum numbers n. This fact allows for nonzero spherical density matrix elements $\rho_{nn'lj}$ with different n and n', off-diagonal in the spherical harmonic oscillator basis.

When the Coulomb interaction is included in the generation of the self-consistent mean field, the spherical density matrix in Eq. (53) is slightly different for protons and neutrons. This amounts to saying that the self-consistent ground-state mean field is not a pure $T = 0$ isospin state, but contains isospin admixtures, mainly $T = 1$ [21], which contribute to the PV $\Delta T = 1$ amplitude. In other words, from the proton and neutron densities $\rho_{nn'lj}^\xi$, $\xi = p, \ n$, one may construct an isoscalar ground-state density $\rho_{nn'lj}^{T=0} = \rho_{nn'lj}^{\xi=p} + \rho_{nn'lj}^{\xi=n}$ and an isovector ground-state density $\rho_{nn'lj}^{T=1} = \rho_{nn'lj}^{\xi=p} - \rho_{nn'lj}^{\xi=n}$ that contribute respectively to the isoscalar and isovector parts of the PV amplitude.

F. Coulomb distortion effects

Another aspect that must be addressed is the Coulomb distortion of the incoming and outgoing electron wave functions. While we are dealing with relatively light nuclei for which Coulomb distortion effects are generally small (at least where the FOM is significant), it is important to perform calculations which fully take into account Coulomb distortion to obtain realistic predictions that can serve as a reference for future experiments. It is also interesting to compare these results with the PWBA calculations described in previous sections. To this end, we follow the standard treatment of Coulomb distortion for elastic PV electron scattering within a partial wave formalism. We solve the Dirac equation for massless electrons in the Coulomb potential generated by the nucleus, closely following the work of refs. [22, 23, 24] to obtain the distorted wave (DW) results.

In Fig. 1 we compare our unpolarized elastic electron scattering cross sections with experimental data for ^{12}C [25, 26, 27, 28, 29], for ^{24}Mg [30, 31], for ^{28}Si [32] and for ^{32}S [32]. For ease of presentation, the cross sections have been transported to a common energy of 400 MeV. Our calculations of cross sections have been obtained from the HF+BCS ground-state densities as described in the previous section. In obtaining these results, no experimental information on, for instance, charge radii, has been employed or fit. In spite of this fact, very good agreement is found up to a scattering angle of 60°, $i.e.,$ a transfer momentum up to around 2 fm^{-1}, which is the region of interest according to the results on FOM to be shown below.

To consider the distorted-wave correction in the PV asymmetries, Eq. (1) has been used, together with Eq. (7) for the asymmetry deviations. The effects of Coulomb distortion and nuclear isospin mixing can be analyzed separately by considering different ingredients in the calculation of the asymmetries in Eq. (7). In Fig. 2 we show the typical distortion effects for 1 GeV electrons in the case of ^{28}Si. The left-hand panel shows isospin-mixing (superscript I) asymmetries in PWBA and when distortions of the electron wave function are taken into account, where the smoothing of the PWBA divergences appears as the most obvious effect of distortion. One must be aware of the fact that without isospin effects and distortion of the electrons, the WNC and EM form factors in Eq. (4) are exactly proportional, and thus the asymmetry follows a very simple $|Q^2|$ dependence (shown by the long dashed line in the left-hand panel of the figure), even at the zeros of the form factor corresponding to the diffraction minima. When isospin effects are considered, the diffraction minima for the WNC and EM form factors occur at slightly different values of q and thus the asymmetry shows extreme variations at the approximate locations of these diffraction minima, as can be seen in the left-hand panel of Fig. 2 (dashed curve). The main effect of the distortion of the electron waves for these light systems is to fill in or to smooth out the diffraction minima, thus severely reducing the amplitude changes of the asymmetry at these diffraction minima, as can also be seen (solid curves) in Fig. 2. Furthermore, the distorting potential introduces asymmetry deviations even when no isospin mixing effects are present in the calculation of the nuclear structure.

In summary, when nuclear isospin mixing is not considered, $i.e.,$ fixing the same proton and neutron densities, the PWBA result shows simply a $|Q^2|$ behaviour, while the results that take into account the distortion of the electron wave function deviate smoothly from this with a dip where the diffraction minimum occurs. When isospin mixing is included, the asymmetry is increased with respect to the non-isospin-mixing case as q approaches the value at the diffraction minima, and it is reduced after the diffraction minima. This behavior is seen both in the PWBA and in the DW calculations.

In the same Fig. 2, the plots in the right-hand panel show asymmetry deviations $\Gamma^{\rm I}$ due to the nuclear isospin mixing obtained replacing $\mathcal{A}/\mathcal{A}^0$ in Eq. (7) by the ratios $\mathcal{A}^{\rm I}_{PW}/\mathcal{A}^0_{PW}$ and $\mathcal{A}^{\rm I}_{DW}/\mathcal{A}^0_{DW}$. In addition we show the pure effect of distortion (ignoring nuclear isospin mixing) obtained from the ratio $\mathcal{A}^0_{DW}/\mathcal{A}^0_{PW}$ and the combined effect of distortion and isospin mixing yielded by using the ratio $\mathcal{A}^{\rm I}_{DW}/\mathcal{A}^0_{PW}$. As one can see in the figure, the effect of distortion is to smooth out the divergences appearing at the position of diffraction minima in PWBA, but anywhere else one sees that the deviations in the asymmetry introduced by isospin mixing effects are very similar both in PWBA and when the distortions are fully taken into account. Analogous results are obtained for ^{12}C, ^{24}Mg and ^{32}S. One should notice that, since we are plotting the absolute value of the asymmetry deviation on a logarithmic scale, zeros of this function appear as downward divergences which remain in the DW calculation.

In the next section we focus the discussion on the results corresponding to the asymmetry deviation. This is defined as the ratio whose numerator is the difference between the asymmetry with isospin mixing and without, and whose denominator is simply the asymmetry with no isospin mixing, where all asymmetries are from full distorted-wave calculations. That is, one has

$$\Gamma^{\rm I}_{DW} \equiv \frac{\mathcal{A}^{\rm I}_{DW}}{\mathcal{A}^0_{DW}} - 1 \,. \tag{54}$$

This deviation may be directly compared with experiment.

It can be seen that this generalized $\Gamma^{\rm I}_{DW}$ yields results that are similar to the PWBA prediction, except for the regions deep in the minima of the cross section. Taking into account that $\mathcal{A}^0_{DW}$ can be computed accurately in a

model-independent way (tables can be produced for each nucleus and different electron energies without difficulty), and the only inputs needed are the (experimental) charge distributions, which are well known for the nuclei studied here, we conclude that the distortion effects will not prevent the determination of isospin mixing effects, provided that the data are compared with a full DW calculation. Indeed, the organization of the asymmetry data according to $\Gamma_{DW}^{\rm I}$ introduced in the equation above may be enough to permit a direct comparison with the simple PWBA predictions for Γ.

It is worth pointing out that the filling of the minima of the cross section is important for the determination of the asymmetry and of the deviations from the non-isospin-mixing prediction, as it is precisely the region near the minima where the isospin mixing effects on the asymmetry are also more evident. The filling of the minima of the form factor and cross section induced by Coulomb distortion will help to make these details of the asymmetry more easily measurable, as the cross section will be much larger in the region of the minima than predicted with the PWBA calculation.

III.   RESULTS

A.   Exploration of basic assumptions

Four even-even, N=Z isotopes have been studied in this work, namely ^{12}C, ^{24}Mg, ^{28}Si and ^{32}S, which for each element are the most abundant isotopes (79% abundance for ^{24}Mg, and higher than 90% for the other isotopes). Furthermore, all targets have reasonably large excitation energies of the first (2^+) excited state, and all but sulfur are suitable in elemental form for high-current electron scattering experiments, as required for a measurement of the PV asymmetry. In our calculations the ground-state deformation is obtained self-consistently. For each nucleus the calculations have been performed using the optimum values of the axially-symmetric harmonic oscillator parameters b and q [17], which define the average length and the axes ratio of the oscillator well. The self-consistent intrinsic proton quadrupole moments are shown in Table I for three different sets of pairing gaps: $\Delta_{\pi,\nu} = 0$ MeV (absence of pairing); $\Delta_{\pi,\nu} = 1$ MeV; and $\Delta_{\pi,\nu}$ as obtained from experimental mass differences [33] of neighboring nuclei through a symmetric five-term formula. These values of the pairing gaps are practically the same for protons and neutrons, namely 4.5 MeV for ^{12}C, 3.13 MeV for ^{24}Mg, 2.88 MeV for ^{28}Si, and 2.17 MeV for ^{32}S. Since these isotopes are relatively light, these pairing gaps are too large because shell effects are not taken into account in the mass formula. The larger pairing gaps tend to give smaller self-consistent deformations. For ^{12}C and ^{32}S we obtain spherical equilibrium shapes in agreement with their vibrational experimental spectra. Table I also includes experimental intrinsic charge quadrupole moments [34]. For ^{24}Mg and ^{28}Si, whose experimental spectra show a rotational band that confirms their deformed shape, the self-consistent values of the quadrupole moment are in better agreement with experiment for the smaller pairing gap values. For this reason, in what follows we focus on results obtained for $\Delta_{\pi,\nu}$ = 1 MeV. Values of $Q_{0\,p} = -21$ fm^2 and $Q_{0\,p} = 52.15$ fm^2 are reported for ^{12}C and ^{32}S respectively in [34]. However, in these two isotopes a ground-state rotational band is by no means recognizable [35], implying that their intrinsic quadrupole ground-state values should be zero and that the ones appearing in [34] do actually correspond to their vibrational 2^+ states. The interpretation of ^{12}C in terms of a 3α structure is gaining more and more experimental support [36]. Obviously this picture is not reducible to a single determinantal function. However, we note the fact that the HF+BCS energy which we obtain as a function of quadrupole deformation shows a shallow minimum around $Q = 0$ for ^{12}C, and this is consistent with that picture. In any case, the final results for PV asymmetries are not very sensitive to the nuclear deformation. This was tested by computing the PV asymmetry for two different shapes of ^{32}S, spherical ($Q_{0p} \sim 0$ fm^2, which is the self-consistent deformation) and prolate ($Q_{0p} \sim 50$ fm^2, which has been fixed by means of a quadrupole constraint in the HF calculation). The results for the two cases were found to be extremely similar, which shows that our predictions are quite independent of the nuclear shape as long as the corresponding self-consistent densities are properly used in the calculations.

In the figures to follow we present the results of isospin mixing for the four isotopes under study, using a SLy4 HF+BCS mean field with $\Delta_{\pi,\nu}=1$ MeV. For comparison, although this is not the primary focus of the present study, we also show results with/without strangeness present, and accordingly a few words are in order concerning what should be regarded to be a sensible value for $\Gamma^{\rm s}$. The experimental value for ρ_s in Eq. (38) is still evolving, given the appearance of new experiments, more detailed analyses of the combined experimental results (see $e.g.,$ [37]) and considerations of complications such as isospin mixing in the nucleon [38] and ^{4}He [5, 39, 40] and the role of two-photon exchange [41]. Presently, from PV electron scattering measurements involving ^{1,2}H and ^{4}He, the value of ρ_s is consistent with zero, and accordingly in the figures we show isospin-mixing results computed with $\rho_s = 0$. The strongest constraint on electric strangeness to date comes from the HAPPEX-He experiment at JLab [8] which yielded the result $G_E^{(s)} = 0.002 \pm 0.014(stat) \pm 0.007(syst)$ at $q = 1.4$ fm^{-1} (corresponding to $Q^2 = 0.077$ (GeV/c)^2), which translates into a range for the electric strangeness parameter used in our parametrization (see Eqs. (38) and (39)) of

$-1.2 \lesssim \rho_s \lesssim +1.4$; to be conservative we have simply added statistical and systematic errors here. Accordingly, in the present study, when referencing our new results to existing estimates of electric strangeness we have adopted the two limit values $\rho_s = \pm 1.5$ as a rough measure when strangeness is present, and $\rho_s = 0$ when it is not — all three of them are essentially consistent with existing knowledge on electric strangeness. Of course, if (when) the amount of electric strangeness is better known from PV electron scattering studies of ^{1,2}H and ^{4}He the present analysis can also easily be updated, both via more refined parametrizations of $G_E^{(s)}$ and in concert with the isospin mixing effects that provide the main focus of the present work. With reference to the results shown below, one should note that the HAPPEX-He PV measurements have been performed in comparable low-q kinematical regions.

For direct comparison with Γ^I we use the Γ^s of Eq. (40). Note that when ρ_s is negative the effects of isospin mixing and strangeness tend to cancel in the low-q region ($q \lesssim 1$ fm^{-1}), whereas the opposite would be true were ρ_s to be positive, which is not ruled out at present. Clearly, in the case where no significant electric strangeness is found in the nucleon the curves with isospin mixing and $\rho_s = 0$ are the appropriate ones. It should also be noted that the strangeness contribution is not very sensitive to details of the nuclear structure (in particular, the approximation of Eq. (40), which is the one plotted in the graphs, is completely independent of the nuclear structure), whereas the isospin contribution does depend on the details of the nuclear structure. For magnetic strangeness (see Eqs. (38) and (39)) following [4] we have assumed that $\mu_s = -0.31$, although the effects in this case are very small and choosing any value that is consistent with present experimental knowledge would lead to negligible differences.

We now begin our discussions of some of the main results of our work, focusing here on an exploration of the basic assumptions made in the present approach, using the case of ^{28}Si to illustrate the various effects under study. In Fig. 3 the left-hand panel shows the total PV asymmetry deviation Γ using the form factor ratio in Eq. (23), together with the isospin mixing contribution Γ^I and the strangeness contribution Γ^s discussed above (as well as below, where the full set of nuclei are inter-related). Discussion of the right-hand panel, which shows the FOM as well as a comparison of plane- and distorted-wave results, is also postponed to later where results for the full set of nuclei are presented. At that point the "doability" of measurements of elastic PV electron scattering is discussed in a little more detail. However, before proceeding with those general results, let us comment on some of the specifics, using the case of ^{28}Si as prototypical.

First, the effect of using different values for the pairing gap in obtaining the asymmetry deviation is shown in Fig. 4, where one can see that the results change very little, even for the larger pairing gap values, as long as the proton and neutron gap values are the same. In conclusion, our results on the PV asymmetry, as shown in the figure, are very stable against changes in the proton and neutron pairing gaps, provided both have the same value. If the proton and neutron pairing gaps were to be notably different, as in one of the examples of Fig. 4, this would lead to a very different structure of the proton and neutron distributions which translates into a different shape for the PV asymmetry deviation.

Secondly, let us discuss the sensitivity of the results to the use of different Skyrme interactions. In Fig. 5 results for ^{28}Si are shown for three different choices, SLy4, Sk3 and SG2. SLy4 force [16] is an example of a recent parametrization and Sk3 [42] is an example of a simple and old force. SG2 [43] has been also widely used in the literature and provides a good description of bulk and spin-isospin nuclear properties as well. Clearly in the low-q region of interest in the present work there is very little sensitivity to the choice of force. The small spread in Γ seen in the figure may be taken as a sort of theory uncertainty with which other competing effects can be compared.

Thirdly, consider the spin-orbit contribution which was introduced as a correction in Eq. (10). While expected to be a small correction, it is important to make sure that this contribution does not confuse the interpretation of the PV asymmetry in terms of isospin mixing. Typically when treating parity-conserving elastic electron scattering the spin-orbit contribution is dominated by isoscalar effects and is known to provide a small correction. However, since the isospin mixing involves a delicate interplay between isoscalar and isovector matrix elements and since the isovector spin-orbit contribution in particular may be sizable (see Eq. (12)): the isovector/isoscalar form factor ratio there is $[2G_M^{(1)} - G_E^{(1)}]/[2G_M^{(0)} - G_E^{(0)}] \cong 11$), this contribution has also been included in the present work for completeness. Results obtained for the PV asymmetry deviation in ^{28}Si performed with and without the spin-orbit correction are almost indistinguishable for momentum transfers lower than about 3.5 fm^{-1}, except near the diffraction minima where the spin-orbit contribution becomes (fractionally) significant and in the dips where $|\Gamma|$ is small anyway. One concludes that, at least in those regions away from the peaks seen in $|\Gamma|$, one should not expect the spin-orbit contributions to lead to confusion when attempting to extract the isospin-mixing behaviour of the PV asymmetry.

Fourthly, a comparison between previous shell-model calculations and our results is now in order. By examining, for instance, Figs. 3 or 7 in DDS together with the present results we immediately see that the effects of isospin mixing are considerably larger here. In the shell-model calculation of DDS, the value of the diagonal density matrix elements for those states below the active shell was the maximum possible occupation of the states in the isoscalar case and zero in the isovector case. For the states in the active shell, only the sum of the density matrix elements was fixed, but not the individual values. All the off-diagonal density matrix elements vanished in the shell-model calculation, but not in the HF calculation for the reasons mentioned above. These off-diagonal matrix elements are the main contributors to the

total isovector form factors obtained in the HF case. In particular, it is of interest to trace back which contributions of the isovector spherical density matrix elements (Eq. (53)) contain the largest major shell mixings. To illustrate this analysis we show in Table II the spherical isovector density matrix elements (diagonal and off-diagonal) for different (l, j) contributions of ^{28}Si. It is found that the off-diagonal isovector density between the harmonic oscillator levels $0d_{5/2}$ and $1d_{5/2}$, i.e., $\rho_{012\frac{5}{2}}^{T=1} = \rho_{012\frac{5}{2}}^{\xi=p} - \rho_{012\frac{5}{2}}^{\xi=n}$, has the largest value, followed by $n = 0, n' = 1$ mixings in $p_{3/2}$ and $p_{1/2}$ ($\rho_{011\frac{3}{2}}^{T=1}$ and $\rho_{011\frac{1}{2}}^{T=1}$ respectively). All of these are normalized to the value of the largest element, $\rho_{012\frac{5}{2}}^{T=1}$. The relative weight of each off-diagonal contribution to the total isovector form factor can change as the momentum transfer varies, and therefore it is necessary in this case to compare the quantities $f_{nn'lj}^{T=1}(q)\, \rho_{nn'lj}^{T=1}$. These are also shown in the table for $q = 0.1$, 0.5 and 1 fm^{-1}. Since the Coulomb monopole operator between two s.h.o. wave functions $f_{nn'lj}(q)$ is proportional to q for off-diagonal contributions, they tend to vanish as $q \to 0$. But for $q \neq 0$, although still relatively small, off-diagonal contributions recover their prominent status determined by the densities.

B.   Inter-comparisons of the full set of nuclei

Now let us turn to general results at low momentum transfers shown in Figs. 3 and 6–9 for the full set of four nuclei. In all cases the left-hand panels show results for the total PV asymmetry deviation $|\Gamma|$ in PWBA for three values of electric strangeness: results with no electric strangeness (solid curve), with $\rho_s = +1.5$ (labeled $+$) and with $\rho_s = -1.5$ (labeled $-$). The strangeness contribution itself (with $|\rho_s| = 1.5$) is shown for reference as a dotted curve. In the right-hand panels the $|\Gamma|$ obtained in plane-wave and distorted-wave cases are compared (solid dark and light lines, respectively) and the FOM obtained either at a fixed scattering angle of $\theta = 10°$ (in PWBA) or at fixed incident energy $\epsilon = 1$ GeV (in DW) (solid and dashed lines, respectively) is presented. The former gives a region around the peak where the FOM reaches reasonable values for the PV deviation to be measured, whereas the latter just shows that the smaller the scattering angle, the larger the FOM. When $q \to 0$ the FOM with fixed scattering angle behaves as q^2, whereas the FOM with fixed incident energy behaves as a constant, this different behavior for $q \to 0$ being apparent in the figures.

To set the scale of "doability" we refer back to our earlier discussions: the ability to measure the PV asymmetry is characterized (at least) by the FOM and at constant angle this increases in going from light nuclei such as ^{4}He to a case such as ^{32}S. Using basic input concerning practical beam currents, electron polarizations, detector solid angles and acceptable running times, in past work (see DDS and also the discussions in Sec. 3.5.2 of [4]), the lower limit was typically chosen to be 0.01, i.e., giving rise at least to a 1% change with respect to the reference (Standard Model) value of the total PV asymmetry. In other words, if something affects the PV asymmetry at (say) the few percent level it can be regarded to be accessible with present technology. Indeed, for elastic PV scattering from He 4% has already been reached [8] and upcoming experiments such as that on Pb aim for even higher precision. Said another way, the peak value of the FOM increases with nuclear species faster than A, while the practical luminosity decreases roughly as $1/A$, making the peak FOM $\times 1/A$ increase by roughly a factor of two in going from ^{4}He (see [4]) to ^{32}S, and thus the "doability" actually increases in going from light to heavier nuclei. Accordingly, in the present study in the figures we have shown where $|\Gamma|$ falls below the 1% level (namely, a bit more challenging than measurements that have already been performed) to indicate the rough division between what is presently within reach for PV electron scattering and what will have to wait for future advances in technology; specifically, in the figures we have indicated with shading where the effects fall below 0.01 and are therefore likely to be inaccessible for the foreseeable future. Table III shows the intervals of momentum transfer (in fm^{-1}) appropriate for the measurement of the isospin-mixing part of the PV asymmetry deviations (or, in other words, when $\rho_s = 0$). These intervals have been chosen so that the deviations are higher than 0.01 and at the same time the FOM at fixed angle is no more than one order of magnitude lower than the maximum value reached at the peak. They are equivalently given in terms of incident electron energies (in MeV). In the case of fixed incident energy, the intervals transform into scattering angle ranges, also shown in the table (in degrees) for $\epsilon = 1$ GeV. These angles are never smaller than 5°, which can be considered an experimental lower bound. As a rough estimate, one can say that in the upper half of the intervals the value of the FOM is very similar no matter what the combination of incident energy and scattering angle used to get the correct transfer momentum.

Note, furthermore, that the FOM is actually only the naive measure (i.e., it characterizes $\delta\mathcal{A}/\mathcal{A}$, as discussed above), whereas, with the isospin-mixing effects increasing with q, a somewhat large value of momentum transfer will actually be the optimal one for experimental study. That is, a compromise must be reached to choose a momentum transfer range where both the PV asymmetry deviation and the FOM are as large as possible. Given the structure of the FOM at fixed angle, decreasing with the momentum transfer due to its cross section dependence, the region of interest corresponds to the first bump of the FOM graph, i.e., between 0 and 1.5 fm^{-1}. Within this transfer momentum range, one has to find a more restrictive region where the PV asymmetry deviation is large enough to be

measurable. The present work is not intended to be a detailed study of experimental possibilities and so we only use the FOM for general guidance. In summary, everything above 10^{-2} in the figures can be considered to be measurable, while the shaded region below this value will be experimentally more challenging.

In Figs. 3 and 6–8 we show in the left-hand panel the PV asymmetry deviations for the three choices of electric strangeness, $\rho_s = -1.5, 0$ and $+1.5$, corresponding roughly to the presently known range of acceptable values. Clearly for positive versus negative electric strangeness the interplay between strangeness and isospin mixing can be quite different: for negative $G_E^{(s)}$ the two effects tend to cancel, whereas for positive $G_E^{(s)}$ they interfere constructively. In the former case this makes the predicted $|\Gamma|$ small, but still potentially accessible, especially in the region at or slightly above $q = 1$ fm^{-1}. In contrast, for positive electric strangeness the asymmetry deviation typically rises above the 10% value in regions where the FOM is peaking — clearly a significant modification of the Standard Model PV asymmetry. One presumes that the ^{4}He case is the best suited to studies of electric strangeness, since isospin mixing is predicted to be much smaller then; however, the interplay of isospin mixing and strangeness seen here for the four nuclei under investigation suggests that these cases could provide information not only about the former effect, but also the latter.

In Figs. 3 and 6–8 we show in the right-hand panel and in a reduced transfer momentum range the isospin-mixing contribution to the asymmetry deviation computed within DW from Eq. (54) and once again in PWBA. The main effect of the DW calculation is to smooth the divergence of the PWBA asymmetry deviation by the appearance of a double-bumped structure. Out of the region of the peaks, the differences between PWBA and DW are seen to be negligible.

Finally, in order to emphasize how the isospin contribution to the PV asymmetry changes as the atomic number increases, we show results from a fully distorted calculation of it in Fig. 9 for the four nuclei under study. We restrict ourselves to the momentum transfer region of most interest for future experiments, as suggested in Table III, and the asymmetry deviation is shown in a non-logarithmic scale. As can be seen in the figure, the isospin contribution in this region of momentum transfer becomes higher as the atomic number increases and typically $|\Gamma|$ goes from a few percent for carbon to well over 10% for the heavier cases. It should be noted that this figure shows effects from isospin mixing alone: if strangeness contributions of order those discussed above were to be present then the total would be modified. For instance, if positive electric strangeness contributions consistent with present experimental limits were present in addition to the isospin-mixing effects discussed in the present work, then the total asymmetry deviations would be roughly twice those seen in the figure, namely, comparatively large effects would be observed.

IV.   CONCLUSIONS

In the present work a new study has been undertaken of the effects expected from isospin-mixing in nuclear ground-state wave functions on elastic parity-violating electron scattering at momentum transfers extending up to about 1.5 fm^{-1}. Four N=Z 0^+ nuclei have been considered, ^{12}C, ^{24}Mg, ^{28}Si, and ^{32}S, each expected to be very close to eigenstates of isospin with $T = 0$ in their ground states. However, as first discussed in [5] (DDS), the Coulomb interaction occurs asymmetrically between pp and pn/nn nucleon pairs in the nucleus, thereby giving rise to small isospin mixing and thus the nuclear ground states considered here have small admixtures with T$\neq$0. While such effects are essentially negligible in the parity-conserving cross section, they can play a measurable role in the parity-violating asymmetry, and accordingly, whether the focus is placed on isospin mixing itself or on how these effects may confuse interpretations of the PV asymmetry in terms of Standard Model tests or with respect to strangeness content in the weak neutral current, it is important to evaluate their influence.

In the older work of DDS a limited-model-space shell model was employed to estimate the isospin mixing and the mixing via the Coulomb interaction was handled perturbatively via a simple two-level approximation. Furthermore, in the study of DDS the idea of using PV elastic electron scattering to determine ground-state neutron distributions as in the case of ^{208}Pb (which forms the basis of the PREX experiment) was put forward; here the focus has been limited to a few special N=Z nuclei and N$\neq$Z cases such as lead have not been re-considered.

In the present work a self-consistent axially-symmetric mean-field approximation with density-dependent effective two-body Skyrme interactions, including Coulomb interactions between pp pairs, has been used in direct determinations of the ground state wave functions. The small differences between the proton and neutron density distributions thereby obtained yield both isoscalar and isovector ground-state Coulomb monopole matrix elements and produce modifications in the PV asymmetry from the model-independent result obtained in the absence of isospin-mixing and strangeness contributions. Additionally, the effects of pairing in this mean-field approximation have also been investigated, as have effects from strangeness contributions in the single-nucleon form factors and from subtle spin-orbit contributions in the Coulomb monopole operators.

A few of the important observations stemming from this study are summarized below.

- In the present work one observes considerably larger effects from isospin mixing than were found in DDS,

especially since here important matrix elements — both diagonal and off-diagonal — are naturally included, whereas in the earlier study the restriction of the shell-model space to a single major shell yielded a special constraint on the q-dependences of the isovector matrix elements.

- Specific influences of nuclear dynamics (different forces, different pairing gaps) and of subtleties in the current operators (spin-orbit effects) were investigated and seen not to affect the PV asymmetry at low-q significantly.

- Results using either plane or distorted electron waves were obtained and, for the relatively light nuclei considered in the present work, their differences were seen to be small at low momentum transfers except in the vicinity of a diffraction minimum where the cross section is also small.

- Kinematic ranges where potential future measurements might be undertaken are discussed by studying both the deviations in the PV asymmetry (the differences seen with/without isospin mixing) and the experimental figure-of-merit. We have shown that the isospin mixing effects considered in this work will have a measurable effect on the asymmetries, even for the light nuclei considered.

- Furthermore, in going from the lightest N=Z nuclei to heavier cases one sees that the asymmetry deviations increase making the isospin-mixing effects all the more evident.

- In exploring the interplay between the isospin-mixing effects and those effects that may arise from electric strangeness contributions one sees an interesting constructive/destructive interference scenario: with positive electric strangeness the two contributions add at low momentum transfers, whereas when negative they subtract. Presently the sign of the electric strangeness form factor is unknown (the form factor is, in fact, consistent with zero) and so such interferences may provide information on isospin mixing, namely the main focus of the present work, but also on strangeness.

Acknowledgments

[1] G. Feinberg, Phys. Rev. D 12 (1975) 3575.
[2] J. D. Walecka, Nucl. Phys. A 258 (1977) 349.
[3] T. W. Donnelly and R. D. Peccei, Phys. Rep. 50 (1979) 1.
[4] M. J. Musolf, T. W. Donnelly, J. Dubach, S. J. Pollock, S. Kowalski and E. J. Beise, Phys. Rep. 239 (1994) 1.
[5] T. W. Donnelly, J. Dubach and I. Sick, Nucl. Phys. A 503 (1989) 589.
[6] C. J. Horowitz, S. J. Pollock, P.A. Souder and R. Michaels, Phys. Rev. C 63 (2001) 025501.
[7] N. Auerbach, Phys. Rep. 98 (1983) 273.
[8] A. Acha, et al., Phys. Rev. Lett. 98 (2007) 032301.
[9] http://hallaweb.jlab.org/parity/prex/
[10] D. Lhuillier Prog. Nucl. Part. Phys. 61 (2008) 183.
[11] J. E. Amaro, J. A. Caballero, T. W. Donnelly, A. M. Lallena, E. Moya de Guerra and Udías, Nucl. Phys. A 602 (1996) 263.
[12] J. E. Amaro, J. A. Caballero, T. W. Donnelly and E. Moya de Guerra, Nucl. Phys. A 611 (1996) 163.
[13] S. Jeschonnek and T. W. Donnelly, Phys. Rev. C 57 (1998) 2438.
[14] M. J. Musolf, R. Schiavilla and T. W. Donnelly, Phys. Rev. C 50 (1994) 2173.
[15] G. Höhler, et al., Nucl. Phys. B 114 (1976) 505.
[16] E. Chabanat, P. Bonche, P. Haensel, J. Meyer and R. Schaeffer, Nucl. Phys. A 635 (1998) 231.
[17] D. Vautherin and D. M. Brink, Phys. Rev. C 5 (19272) 626; D. Vautherin, Phys. Rev. C 7 (1973) 296.
[18] E. Moya de Guerra, P. Sarriguren, J. A. Caballero, M. Casas and D. W. L. Sprung, Nucl. Phys. A 529 (1991) 68.
[19] E. Moya de Guerra, Phys. Rep. 138 (1986) 293.
[20] A. Zaringhalam and J. W. Negele, Nucl. Phys. A 288 (1977) 417.
[21] R. Álvarez-Rodríguez, E. Moya de Guerra and P. Sarriguren, Phys. Rev. C 71 (2005) 044308.

[22] C. J. Horowitz, Phys. Rev. C 57 (1998) 3430.

[23] G. Rufa, Nucl. Phys. A 384 (1982) 273.

[24] A. N. Antonov, D.N. Kadrev, M.K. Gaidarov, E. Moya de Guerra, P. Sarriguren, J.M. Udias, V.K. Lukyanov, E.V. Zemlyanaya and G.Z. Krumova, Phys. Rev. C 72 (2005) 044307.

[25] I. Sick and J. S. McCarthy, Nucl. Phys. A 150 (1970) 631.

[26] J. A. Jansen, R. T. Peerdeman and C. deVries, Nucl. Phys. A 188 (1972) 337.

[27] G. Fey, Thesis, TH Darmstadt, 1973.

[28] L. S. Cardman, J. W. Lightbody, S. Penner, W. P. Trower and S. F. Williamson, Phys. Lett. B 91 (1980) 203.

[29] W. Reuter, Thesis KPH Mainz, 1981.

[30] G. C. Li, I. Sick and M. R. Yearian, Phys. Rev. C 9 (1974) 1861.

[31] E. W. Lees, C. S. Curran, T. E. Drake, W. A. Gillespie, A. Johnson and R. P. Singhal, J. Phys. G 2 (1976) 105.

[32] G. C. Li, I. Sick and M. R. Yearian, Phys. Lett. B 37 (1971) 282.

[33] G. Audi, O. Bersillon, J. Blachot and A. H. Wapstra, Nucl. Phys. A 729 (2003) 3.

[34] P. Raghavan, Atomic and Nuclear Data Tables 42 (1989) 189; N.J. Stone, Table of Nuclear Moments (2001) www.nndc.bnl.gov/nndc/stone_moments

[35] Table of Isotopes, 8 th. ed., 1999 update (eds. R.B. Firestone and V.S. Shirley) (Wiley Interscience, 1999)

[36] H. Fynbo, et al., Science 433 (2005) 136.

[37] D. B. Leinweber, S. Boinepalli, A. W. Thomas, P. Wang, A. G. Williams, R. D. Young, J. M. Zanotti and J. B. Zhang, Phys. Rev. Lett. 97 (2006) 022001.

[38] B. Kubis and R. Lewis, Phys. Rev. C 74 (2006) 015204.

[39] S. Ramavataram, E. Hadjimichael and T. W. Donnelly, Phys. Rev. C 50 (1994) 1175.

[40] M. Viviani, R. Schiavilla, B. Kubis, R. Lewis, L. Girlanda, A. Kievsky, L.E. Marcucci and S. Rosati, Phys. Rev. Lett. 99 (2007) 112002.

[41] H. Q. Zhou, C. W. Kao and S. N. Yang, Phys. Rev. Lett. 99 (2007) 262001.

[42] M. Beiner, H. Flocard, N. Van Giai and P. Quentin, Nucl. Phys. A 238 (1975) 29.

[43] N. Van Giai and H. Sagawa, Phys. Lett. B 106 (1981) 379.

TABLE I: Theoretical (deformed HF or HF+BCS) and experimental [34] intrinsic proton quadrupole moments $Q_{0\,p}$ [fm^2] of the ground-state rotational band in each of the isotopes under study, together with the corresponding pairing gap $\Delta_{\pi,\nu}$ used in the HF+BCS (coul.+pair.) calculation.

Isotope	$\Delta_{\pi,\nu} = 0$	$\Delta_{\pi,\nu} = 1$ MeV	$\Delta_{\pi,\nu}$ from mass diff.	Exp. [34]
^{12}C	~ 0	~ 0	~ 0	-
^{24}Mg	56.67	54.70	38.54	58.1
^{28}Si	-45.35	-43.41	-28.62	-57.75
^{32}S	~ 0	~ 0	~ 0	-

TABLE II: Main single-particle (l, j) components of the total HF+BCS ground-state isovector density $\rho_{nn'lj}^{T=1} = \rho_{nn'lj}^{\xi=p} - \rho_{nn'lj}^{\xi=n}$ and Coulomb monopole form factor $f_{nn'lj}(q)\,\rho_{nn'lj}^{T=1}$ (at $q = 0.1$, 0.5 and 1 fm^{-1}) of ^{28}Si, for different combinations of radial quantum numbers n, n'. Results are normalized to the largest contribution and only the absolute values are given, not the signs. The largest value for each (l, j) component is written in boldface.

l	j	n	n'	$\rho_{nn'lj}^{T=1}$	$f_{nn'lj}\,\rho_{nn'lj}^{T=1}$		
					$q = 0.1$ fm^{-1}	$q = 0.5$ fm^{-1}	$q = 1$ fm^{-1}
		0	0	0.058	**0.208**	0.229	0.145
		0	1	0.168	0.005	0.136	**0.346**
0	1/2	0	2	0.052	0.000	0.005	0.048
		1	1	0.028	0.100	0.079	0.024
		1	2	**0.203**	0.011	**0.244**	0.304
		0	0	0.093	**0.335**	0.309	0.078
		0	1	**0.349**	0.013	**0.329**	**0.555**
1	1/2	0	2	0.048	0.000	0.006	0.048
		1	1	0.093	0.330	0.217	0.047
		1	2	0.018	0.001	0.023	0.018
		0	0	0.184	**0.662**	**0.610**	0.016
		0	1	**0.628**	0.024	0.592	**1.000**
1	3/2	0	2	0.137	0.000	0.018	0.137
		1	1	0.186	0.659	0.434	0.094
		1	2	0.031	0.002	0.040	0.032
		0	0	0.044	**0.156**	**0.119**	0.007
		0	1	**0.061**	0.003	0.061	**0.060**
2	3/2	0	2	0.008	0.000	0.001	0.007
		1	1	0.001	0.004	0.002	0.000
		1	2	0.002	0.000	0.002	0.001
		0	0	0.142	0.506	0.386	0.024
		0	1	**1.000**	0.045	**1.000**	0.986
2	5/2	0	2	0.048	0.000	0.008	0.044
		1	1	0.284	**1.000**	0.541	0.075
		1	2	0.379	0.003	0.049	0.021

TABLE III: Momentum transfer intervals (in fm^{-1}) appropriate for the measurement of the isospin-mixing contribution (*i.e.*, $\rho_s = 0$) to the PV asymmetry deviation, chosen so that it is higher than 0.01 and the FOM at $\theta=10°$ is no more than one order of magnitude lower than its maximum value (see Figs. 3, 6 – 8). Corresponding ranges of incident energy ϵ at $\theta=10°$ (in MeV) and scattering angle θ at E=1 GeV (in degrees) are also given.

Isotope	for Γ^{I}
^{12}C	$0.74 \leq \mathrm{q} \leq 1.42$
	$838 \leq \epsilon \leq 1607$
	$8.38 \leq \theta \leq 16.07$
^{24}Mg	$0.51 \leq \mathrm{q} \leq 1.10$
	$577 \leq \epsilon \leq 1245$
	$5.77 \leq \theta \leq 12.45$
^{28}Si	$0.48 \leq \mathrm{q} \leq 1.08$
	$543 \leq \epsilon \leq 1222$
	$5.43 \leq \theta \leq 12.22$
^{32}S	$0.45 \leq \mathrm{q} \leq 1.05$
	$509 \leq \epsilon \leq 1188$
	$5.09 \leq \theta \leq 11.88$
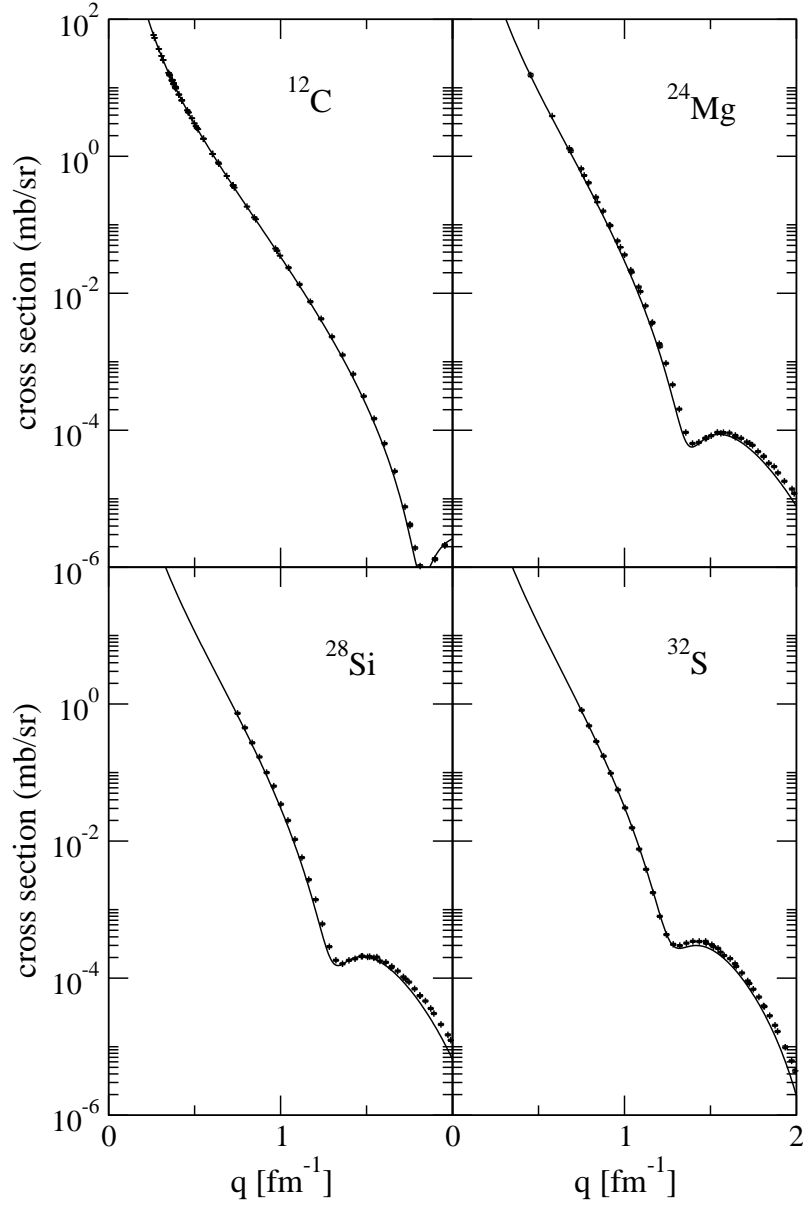
FIG. 1: Experimental data with error bars and theoretical (solid line) electron-nucleus cross section. Ground-state nuclear densities are obtained from a HF(SLy4)+BCS($\Delta_{\pi,\nu}$= 1 MeV) distorted wave calculation for 400 MeV electrons.
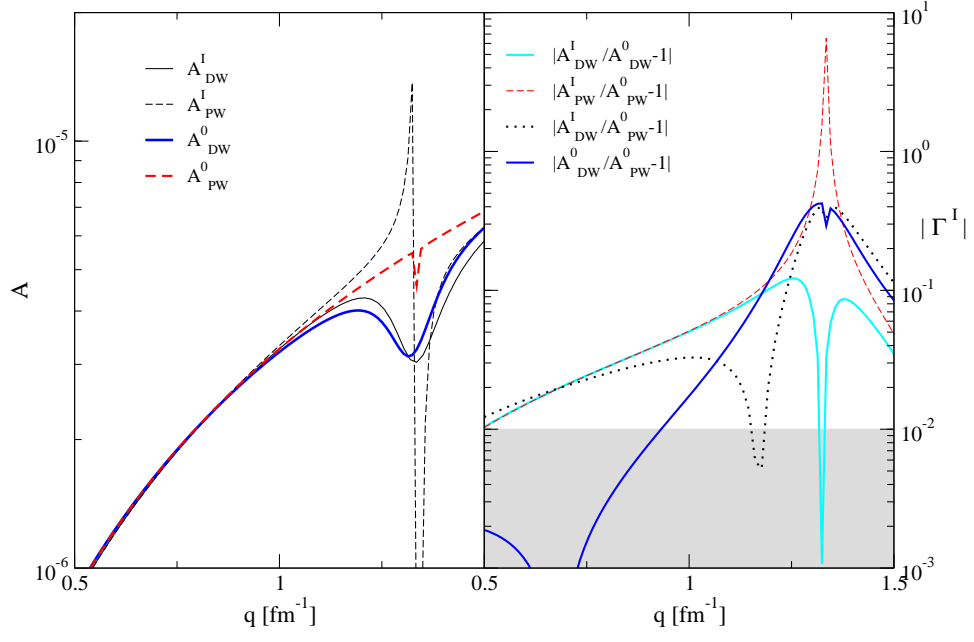
FIG. 2: (Color online) Left-hand panel: PV asymmetry for ^{28}Si allowing for nuclear isospin mixing in PWBA and in the fully distorted calculation (PW^I and DW^I) and in the non-isospin-mixing case by constraining $\rho^p = \rho^n$ (PW^0 and DW^0). Right-hand panel: Asymmetry deviations for ^{28}Si: due to pure isospin mixing effects in DW (solid line) and in PWBA (dashed line), due to isospin mixing and distortion effects together (dotted line) and due to distortion effects only (thick solid line).
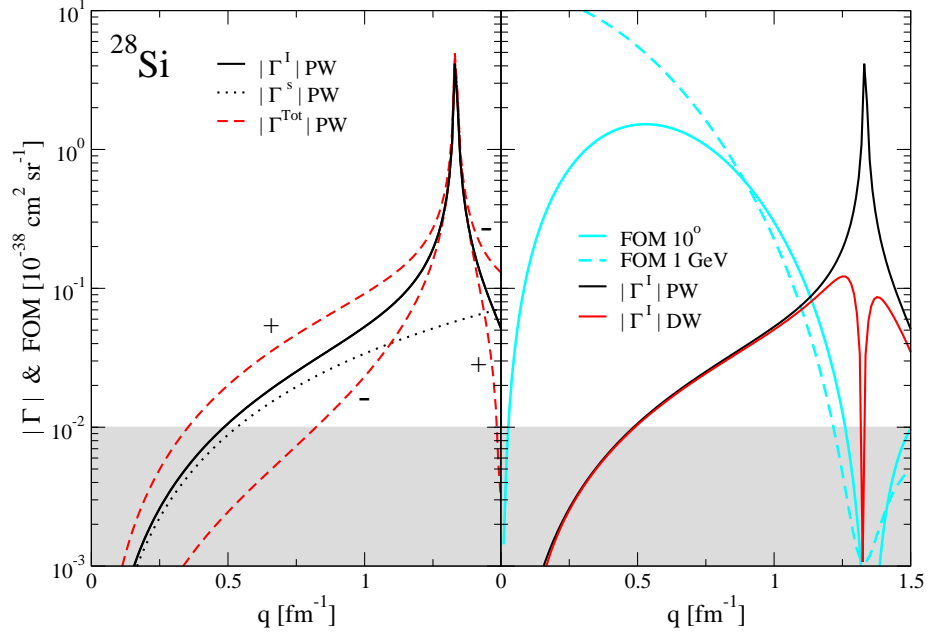
FIG. 3: (Color online) Left-hand panel: total PV asymmetry deviation (dashed line) for ^{28}Si from a HF(SLy4)+BCS($\Delta_{\pi,\nu}=1$ MeV) calculation in PWBA with a strangeness contribution using two values of ρ_s, namely ± 1.5, together with the corresponding nucleon strangeness content (with $\rho_s=1.5$) contribution Γ^s (dotted line). Total PV asymmetry for $\rho_s=0$, *i.e.*, the pure isospin-mixing contribution, is also shown (solid line). Right-hand panel: The latter curve again (solid dark line) and the same result but in DW with 1 GeV electrons (solid light line), together with the FOM corresponding to the total PV asymmetry for a fixed scattering angle of 10° (thick solid line) and for a fixed incident energy of 1 GeV (thick dashed line). The shaded region below $\Gamma=0.01$ is experimentally challenging, in contrast to the rest of the plot which, as discussed in the text, may be considered to be accessible with present technology.
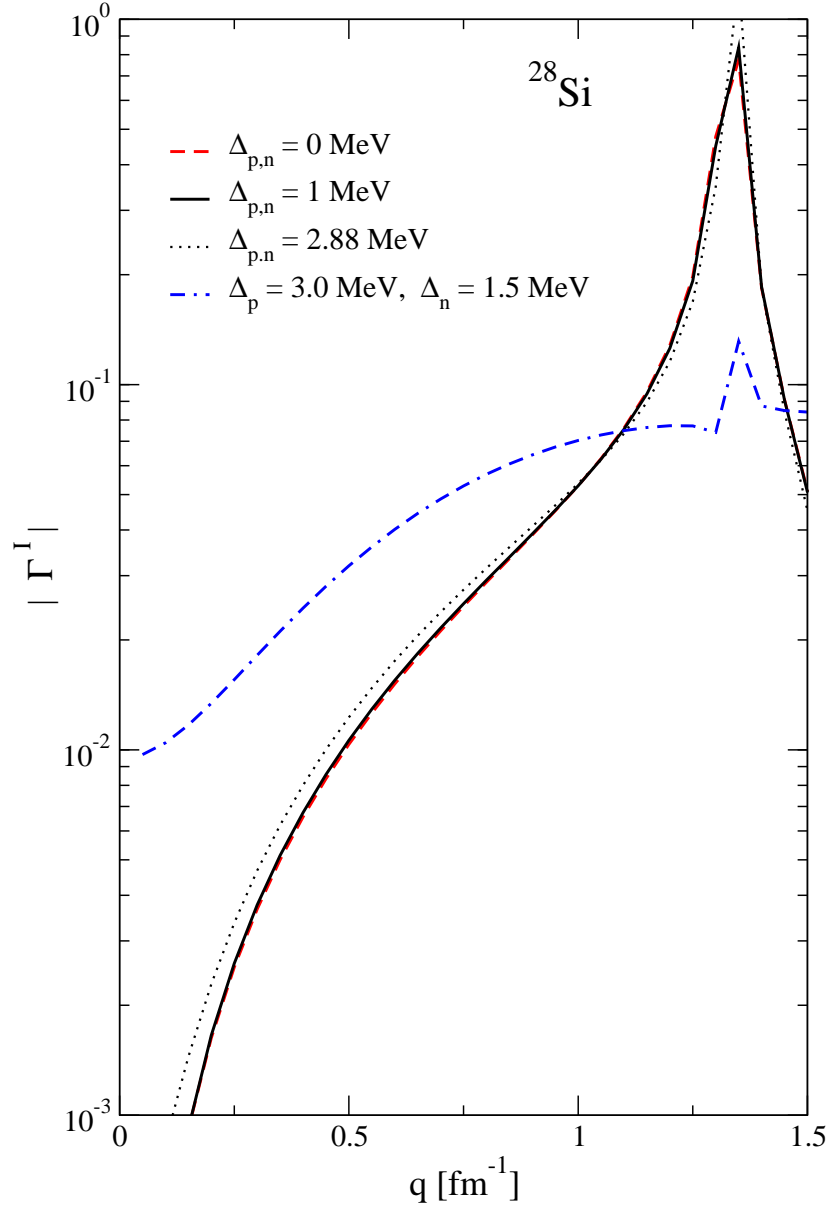
FIG. 4: (Color online) Isospin mixing contribution to the PV asymmetry deviation in ^{28}Si from a HF(SLy4) (or HF+BCS) calculation for three values of the pairing gap: $\Delta_{\pi,\nu}= 0$ MeV (solid line), $\Delta_{\pi,\nu}= 1$ MeV (dashed line) and $\Delta_{\pi,\nu}= 2.88$ MeV (dotted line). Also shown are results for different Δ_π and Δ_ν values (dash-dotted line).
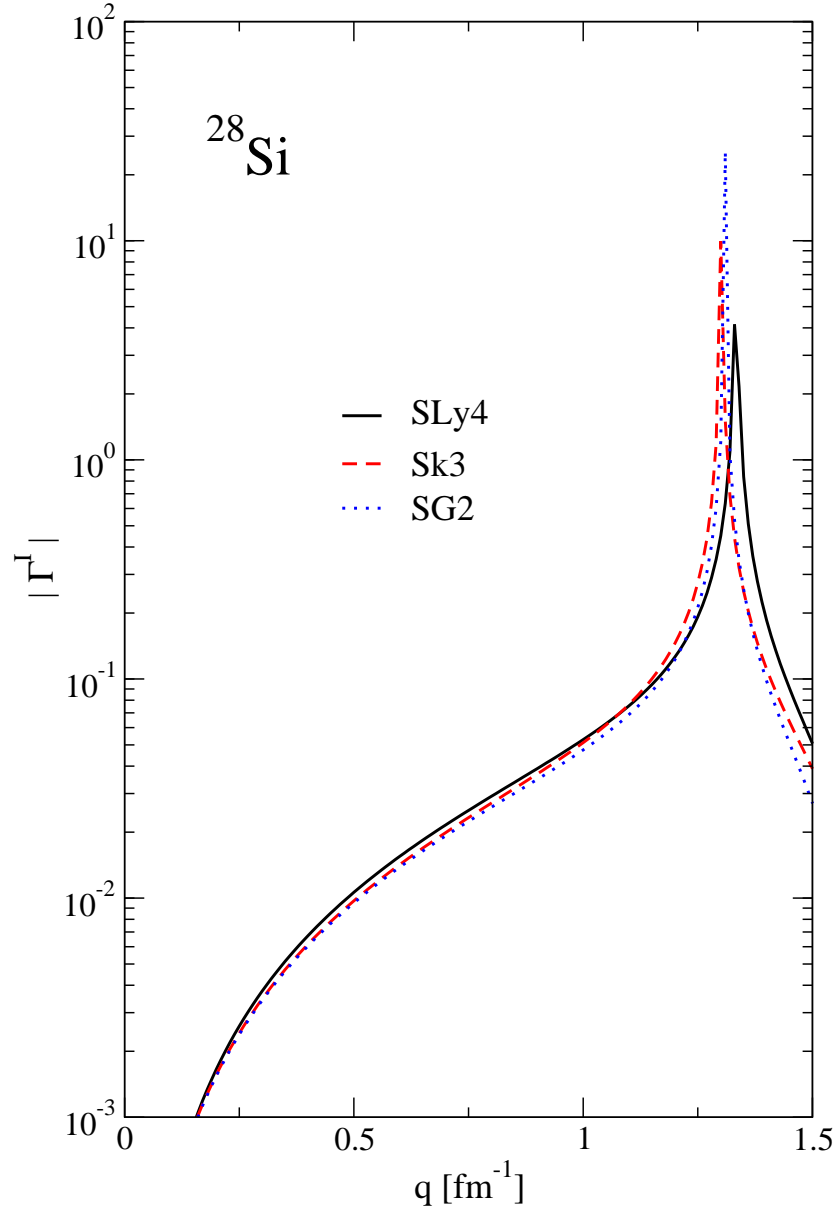
FIG. 5: (Color online) Isospin mixing contribution to the PV asymmetry deviation in ^{28}Si from a HF+BCS calculation for three Skyrme forces: SLy4 (solid line), Sk3 (dashed line) and SG2 (dotted line).
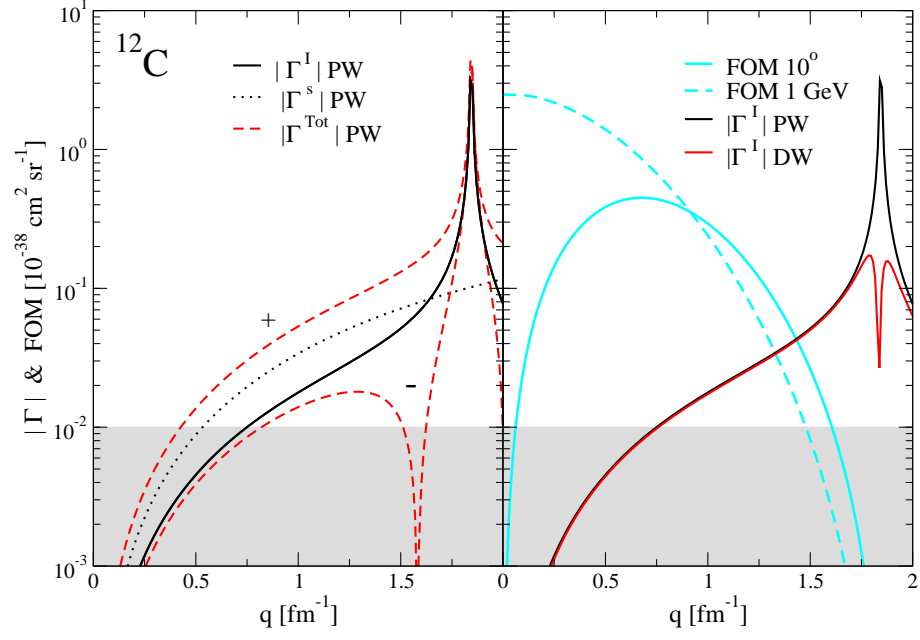
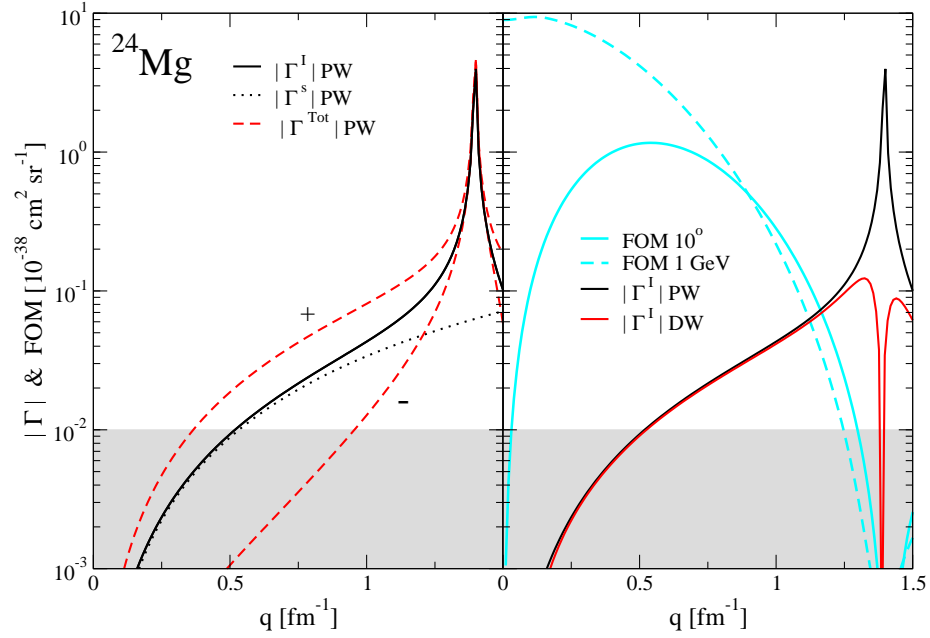FIG. 6: (Color online) As for Fig. 3, but now for ^{12}C.
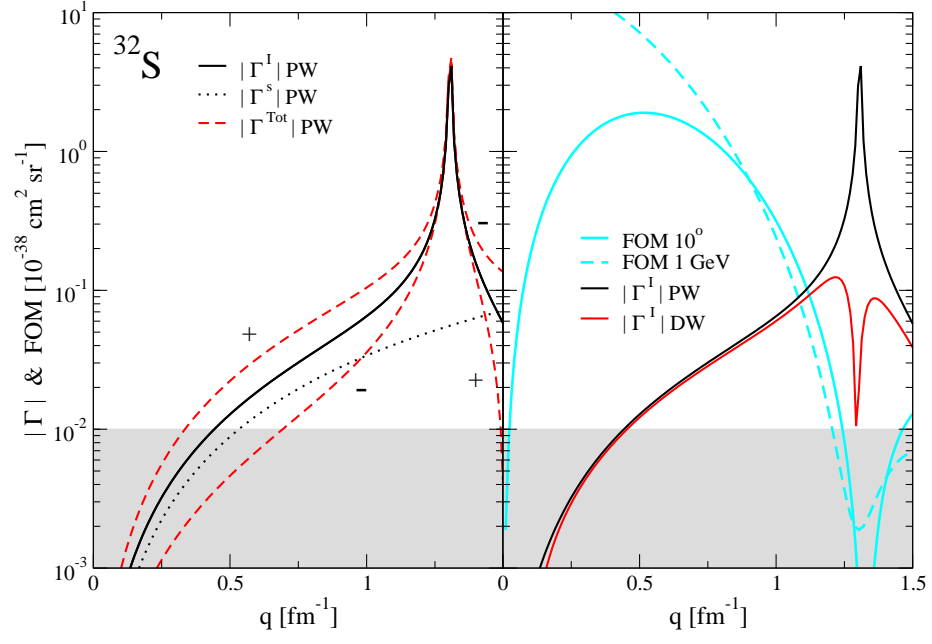

FIG. 7: (Color online) As for Fig. 3, but now for ^{24}Mg.
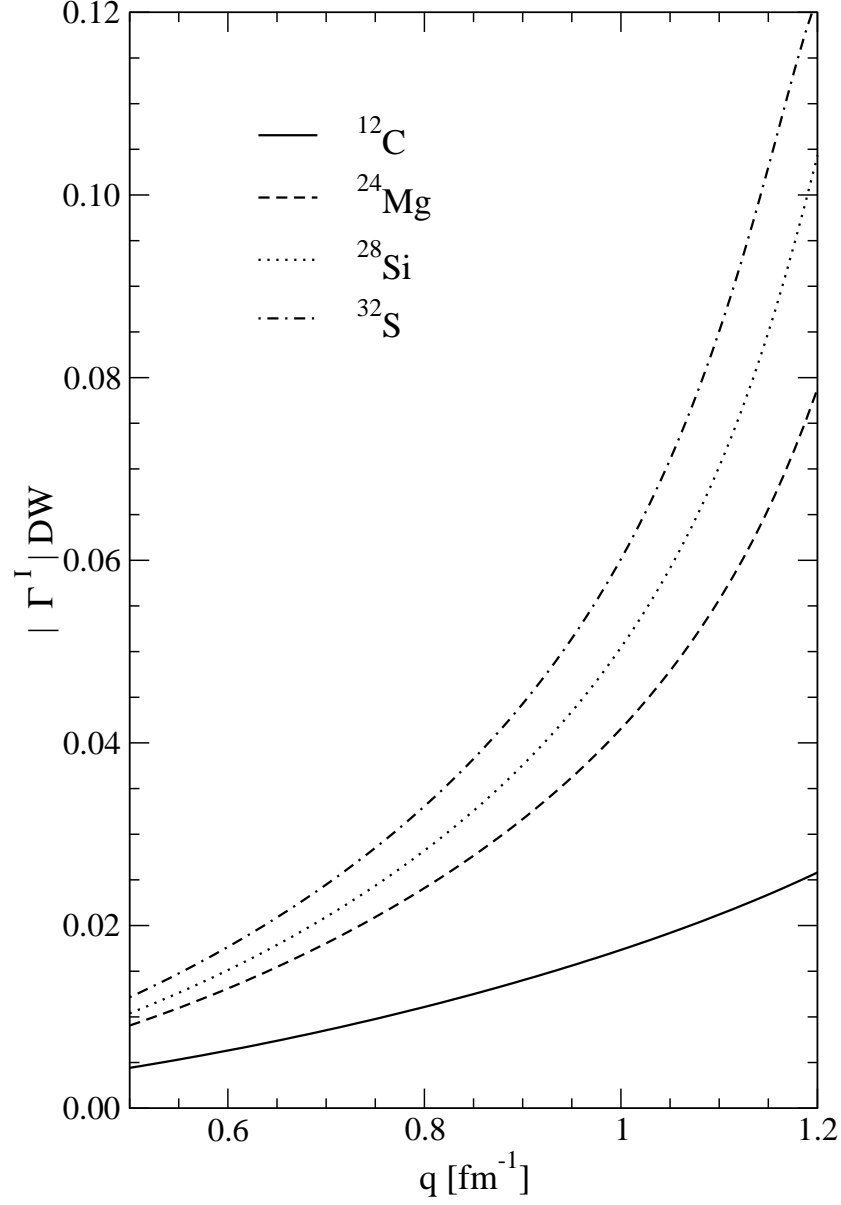
FIG. 8: (Color online) As for Fig. 3, but now for ^{32}S.

FIG. 9: Isospin mixing contribution to the PV asymmetry deviation Γ^I for the four nuclei under study from a HF(SLy4)+BCS($\Delta_{\pi,\nu}= 1$ MeV) calculation in DW for 1 GeV electrons, in the momentum transfer region of most experimental interest. No strangeness contributions are included here.